Journal of Electromagnetic Waves and Applications

Publication details, including instructions for authors and subscription information:
http://www.tandfonline.com/loi/tewa20

Extraction of jet engine modulation component weakly present in measured signals for enhanced radar target recognition

Ji-Hoon Park[a], Woo-Yong Yang[a], Jun-Woo Bae[b], Seong-Cheol Kang[b], Chan-Hong Kim[c] & Noh-Hoon Myung[a]

[a] Department of Electrical Engineering, Korea Advanced Institute of Science and Technology (KAIST), 335 Gwahangno, Yuseong-gu, Daejeon 305-701, Korea

[b] Samsung Thales, Sampyong-Dong, Bundang-Gu, Seongnam 463-400, Korea

[c] Agency for Defense Development, Yuseong P.O. Box 35-3, Daejeon, Korea

Published online: 24 Mar 2014.

To cite this article: Ji-Hoon Park, Woo-Yong Yang, Jun-Woo Bae, Seong-Cheol Kang, Chan-Hong Kim & Noh-Hoon Myung (2014) Extraction of jet engine modulation component weakly present in measured signals for enhanced radar target recognition, Journal of Electromagnetic Waves and Applications, 28:8, 963-975, DOI: 10.1080/09205071.2014.899168

To link to this article: http://dx.doi.org/10.1080/09205071.2014.899168

Journal of Electromagnetic Waves and Applications, 2014
Vol. 28, No. 8, 963–975, http://dx.doi.org/10.1080/09205071.2014.899168

Extraction of jet engine modulation component weakly present in measured signals for enhanced radar target recognition

Ji-Hoon Park[a]*, Woo-Yong Yang[a], Jun-Woo Bae[b], Seong-Cheol Kang[b], Chan-Hong Kim[c] and Noh-Hoon Myung[a]

[a]*Department of Electrical Engineering, Korea Advanced Institute of Science and Technology (KAIST), 335 Gwahangno, Yuseong-gu, Daejeon 305-701, Korea;* [b]*Samsung Thales, Sampyong-Dong, Bundang-Gu, Seongnam 463-400, Korea;* [c]*Agency for Defense Development, Yuseong P.O. Box 35-3, Daejeon, Korea*

(*Received 25 August 2013; accepted 24 February 2014*)

This study presents a method for extracting the jet engine modulation (JEM) component weakly present in the radar received signal. First, the analytic form of the complicated measured signal is decomposed into intrinsic mode functions (IMFs) via complex empirical mode decomposition (CEMD). Then, the extracted IMFs are combined to reconstruct the JEM component based on the signal eccentricity, which serves as assessing the JEM micro-Doppler contribution to the signal. Applying these techniques to the measured raw signals demonstrate that the proposed extraction method significantly improves the clarity of the JEM analysis and is expected to be useful for enhanced radar target recognition.

Keywords: complex empirical mode decomposition (CEMD); jet engine modulation (JEM); micro-Doppler; radar target recognition; signal eccentricity

1. Introduction

Jet engine modulation (JEM) effect, one of the micro-Doppler (m-D) phenomena induced by a rotating jet engine turbine, is a representative means for radar target recognition.[1–5] By providing additional and unique information on the equipped jet engine, the JEM effect is complementary to other existing methods, such as range profiles and radar imagery.[6,7] However, most real radar signals from aircraft targets always contain not only the JEM component but also components scattered from the rigid aircraft structure, such as the aircraft body or the outer wall enclosing the jet engine turbine. Thus, the JEM component may become weak in relation to the body returned component when the structural scattering is emphatic. Since this situation can lead to degradation of JEM recognition performance, it is important to extract the weakly present JEM component for enhanced target recognition.

In recent years, extraction of the m-D component has attracted great research attention and various techniques have been proposed for accurate parameter estimation.[8–15] Because they chiefly focused on enhancing the quality of radar images by removing the interfering m-D component, the m-D component was assumed to account for a substantially large portion of the radar received signal. However, despite

*Corresponding author. Email: dydynoel@kaist.ac.kr

importance of the JEM in the radar target recognition, there has been a lack of work on extracting the JEM component, which weakly exists in the measured signal.

This study proposes a method for effectively extracting the JEM component. We employed complex empirical mode decomposition (CEMD) [16–18] because of its fully data-driven characteristics, intuitiveness for discriminating the m-D component and signal extraction performance. According to [19], CEMD can extract the signal component with amplitude as much as 20 dB lower than that of another component for a sufficient frequency distance. Considering complexity of signals measured from jet engines,[8] we applied CEMD to the signal analytic form [20] in which the composition of frequency components could be simplified. Then, in order to reconstruct the JEM component, signal eccentricity [21,22] assessed the JEM contribution and indicated the desirable combination of intrinsic mode functions (IMFs) extracted from CEMD. After applying the proposed method to the signals measured from the experimental jet engine model, the clarity of the JEM analysis was significantly improved by including only the JEM-related IMFs. Note that in this study, the JEM component is defined as being weakly present in the radar received signal when the JEM spectral lines have the amplitude at least 10 dB lower than that of the body returned component.

2. Basic techniques for extracting the weak JEM component

2.1. Signal eccentricity concept

Based on scattering points, the radar signal returned from both the rotating engine turbine and the aircraft structure can be conceptually modeled as the sum of the m-D component $s_{mD}(t)$ with the sinusoidal phase and the body returned component $s_{body}(t)$ with the linear phase such that [12–14]

$$s(t) = s_{mD}(t) + s_{body}(t) = \exp\left[j\frac{4\pi R_{mD}}{\lambda}\sin(\omega_{mD}t)\right] + \exp\left[j\frac{4\pi R_{bd}}{\lambda}\omega_{bd}t\right] \tag{1}$$

where λ is the radar wavelength, R_{mD} and R_{bd} are the rotation radius of the micromotion part and the distance from the target geometrical center to a scattering point on the target body, respectively. ω_{mD} and ω_{bd} are the angular speeds of the rotating part and the target. Note that the second term in (1) was approximated by the small accumulation angle assumption,[12] namely, $\omega_{bd}t \ll 1$. It should be emphasized that since $\omega_{mD} \gg \omega_{bd}$, $s_{mD}(t)$ rotates much more rapidly than $s_{body}(t)$ in the complex-time domain composed of real, imaginary, and time axes.

To quantitatively estimate the m-D contribution to $s(t)$, this study employs signal eccentricity as follows [21,22]:

$$\varepsilon = \sqrt{\left|\frac{E[\mathbf{s}\cdot\mathbf{s}^T]}{E[\mathbf{s}\cdot\mathbf{s}^H]}\right|} \tag{2}$$

where $\mathbf{s} = s(t)$ and $E[\bullet]$ is the expectation operator. ε measures how far $\mathbf{s}$ deviates from circularity with respect to the central axis of the complex plane and ranges between 0 for pure circular polarization and 1 for pure linear polarization. For the limited dwell time of JEM measurement,[1,2] the slowly rotating $s_{body}(t)$ will appear to be linearly polarized as opposed to the rapidly rotating $s_{mD}(t)$, which will retain its circularly rotating behavior. Therefore, when the body returned component strongly overlaps with the m-D, $s(t)$ has a large eccentricity value since it deviates from the central axis. We can also predict that the eccentricity decreases for the m-D extracted from $s(t)$.

Figure 1(a) depicts both $s_{mD}(t)$ and $s_{body}(t)$ when R_{mD}, R_{bd}, ω_{mD}, and ω_{bd} are given as 0.25 m, 2 m, 10 rad/s, and 0.02 rad/s, respectively. For a wavelength of 0.03 m and during a dwell time of 0.1 s, the eccentricity of $s_{body}(t)$ is 0.77 whereas that of $s_{mD}(t)$ is only 0.07 because $s_{mD}(t)$ maintains the circular rotation around the central axis. Consequently, as shown in Figure 1(b), $s(t)$ rotates around $s_{body}(t)$ and has a relatively large eccentricity of 0.56. This illustration suggests that signal eccentricity can be a good metric for assessing the JEM m-D contribution.

2.2. *Analytic form of a complex-valued signal*

In practice, the raw signal $s(t)$ measured from the real jet engine consists of complicated frequency components.[1–3,8] Thus, instead of $s(t)$, we apply CEMD to its analytic form $s_a(t)$ discussed in the field of vector sensors [20] as follows:

$$s_a(t) = \begin{cases} V_x - H\{V_y\} + j[H\{V_x\} + V_y], & \text{positive form} \\ V_y - H\{V_x\} - j[H\{V_y\} + V_x], & \text{negative form} \end{cases} \tag{3}$$

where V_x and V_y are the real part and the imaginary part of the original signal $s(t)$, and $H\{\bullet\}$ denotes the Hilbert transform. The positive and negative forms make $s(t)$ concentrate on the positive and negative frequency components, respectively. Although $s_a(t)$ takes advantage of only the one-sided band, it can have more simplified frequency components by excluding a number of extraneous spectral lines, such as the spurious components caused by intermodulation between turbine rotor stages.

To illustrate the advantage of the analytic transformation in dealing with the complicated signal, we examine the signal measured from the experimental jet engine [3] with a rotation speed of 60.1 RPM and a radar aspect angle of 60°. Figure 2 shows the spectra of the signal and its analytic forms. As observed in Figure 2(a), the raw spectrum shows a waveform with a number of spectral lines. However, the frequency components in Figure 2(b) and (c) are simplified and the remaining spectral lines are approximately twice magnified. Since either a positive or a negative form should be applied to CEMD, we select the one with less eccentricity, which better retains the circularly rotating characteristic. Here, the positive $s_a(t)$ is chosen since it has an eccentricity of 0.972 less than that of the negative $s_a(t)$ of 0.990, and thus shows the modulated spectral lines more clearly. The analytic form can raise the possibility of accurately extracting the JEM component from the complicated measured signal.

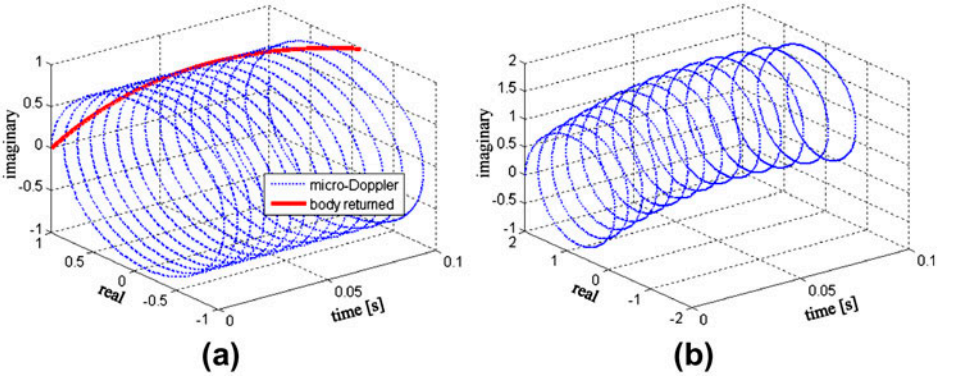

Figure 1. Signal rotating behavior in the complex-time domain. (a) $s_{body}(t)$ and $s_{m\text{-}D}(t)$, and (b) radar received signal $s(t)$.

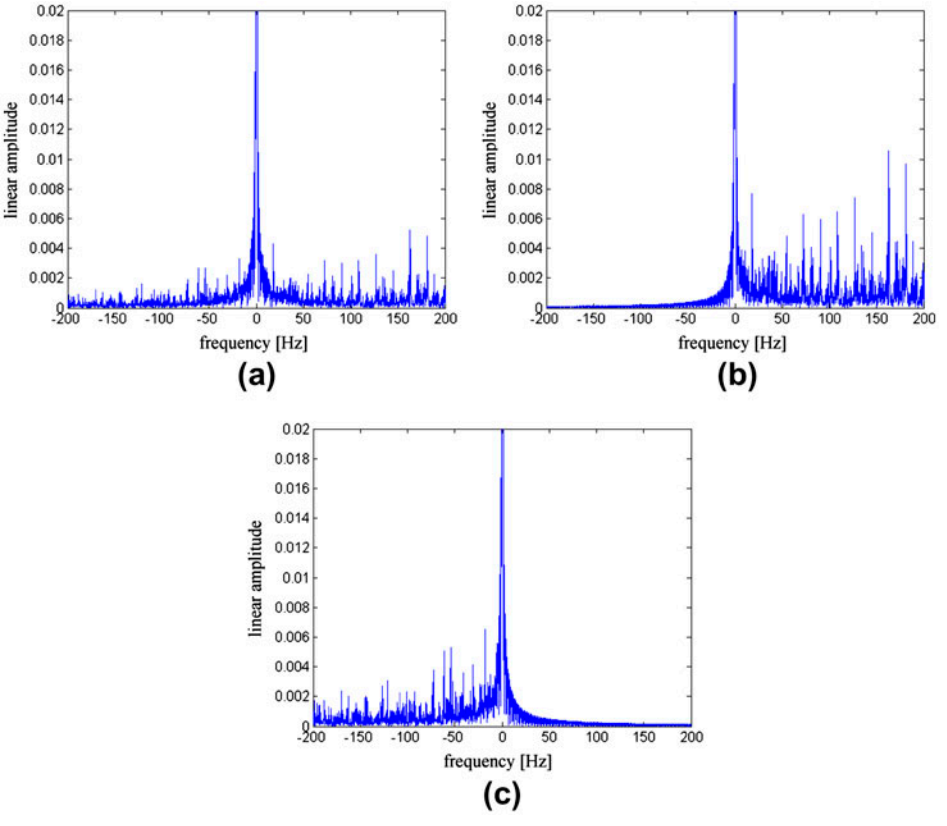

Figure 2. Illustration of signal spectra. (a) Measured raw signal $s(t)$, (b) positive analytic form $s_a(t)$ and (c) negative analytic form $s_a(t)$.

2.3. *JEM reconstruction with CEMD and signal eccentricity*

CEMD [16–18] is the complex extension of the original EMD [23] and iteratively separates the rapidly rotating components from slowly rotating components. Each decomposed component is referred to as an IMF. Brief procedures of CEMD are given as follows [16]:

(1) Projection of $s_a(t)$ on a given set of directions $\varphi_k = 2\pi k/N$, where $k = 1, \ldots, N$

$$p_{\varphi_k}(t) = \mathrm{Re}(s_a(t)e^{-j\varphi_k}) \tag{4}$$

(2) Extraction of the locations $\{t_j^k\}$ at the maxima of $p_{\varphi_k}(t)$
(3) Cubic spline interpolation of the set $\{t_j^k, s_a(t_j^k)\}$ to obtain the envelope curve $e_{\varphi_k}(t)$
(4) Calculation of the mean of all envelope curves using

$$m(t) = \frac{1}{N}\sum_{k=1}^{N} e_{\varphi_k}(t) \tag{5}$$

(5) Subtraction of $m(t)$ from $s_a(t)$ and designation of the result as a complex IMF

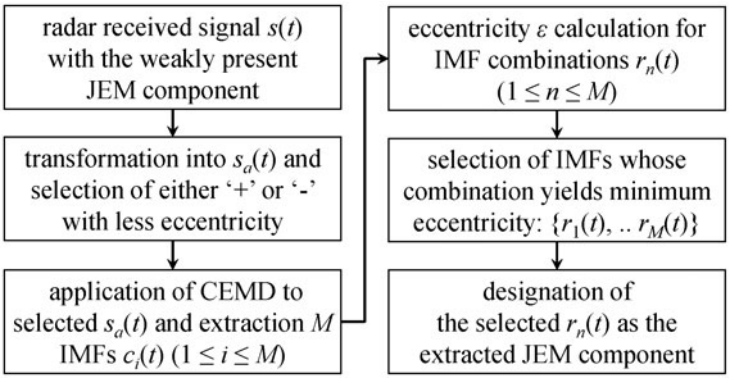

Figure 3. Flow chart of the proposed method for extracting the weak JEM component present in the measured raw signal.

Since each derived IMF does not directly represent the motion dynamics, a standard for combining IMFs relevant to the JEM component needs to be constructed. Although the number of zero-crossings was employed for separating the m-D in radar imaging, [12] it may become ambiguous if there is no drastic change in the zero-crossing numbers along the extracted IMFs. In this study, we select the JEM-related IMFs based on the minimum eccentricity condition. Using the relation between signal composition and eccentricity, the IMF combination with the minimum eccentricity condition is expected to best characterize the rapidly rotating JEM component.

Figure 3 summarizes the proposed extraction method. First, CEMD decomposes the selected analytic form of the signal into M IMFs $c_i(t)$ where i denotes the index of the IMF extraction order. Then, the eccentricity ε is calculated for the IMF combination $r_n(t)$, which sequentially combines IMFs by the order of degree of rotation as follows:

$$r_n(t) = \sum_{i=1}^{n} c_i(t), \quad 1 \le n \le M \tag{6}$$

Note that $r_n(t)$ becomes the same as $s_a(t)$ when n is equal to M. Finally, we designate $r_n(t)$ with the minimum eccentricity value as the extracted JEM component.

2.4. *Illustrative example*

In this subsection, an illustrative example of the proposed method is provided to give an insight into the weakly present JEM component and its extraction process. We examine a signal from a shooting and bouncing rays (SBR)-based simulation of a realistic jet engine CAD model. The detailed information is available in [4], and simulation parameters are identical to those in [4] except for the radar aspect angle. Considering that the JEM is typically observable from 0° to 60°,[1] the signal with an aspect angle of 10° was used in [4]. However, the angle was given as 80° in this illustration because the obliquely incident signal may be blocked by the outer wall of the jet engine, and thus, weak scattering from the rotating turbine may occur. In contrast to Figure 4(a) exhibiting the JEM spectrum of 10°, Figure 4(b) shows the JEM spectrum of 80° where the JEM spectral lines have significantly low amplitude. In addition, it can be shown

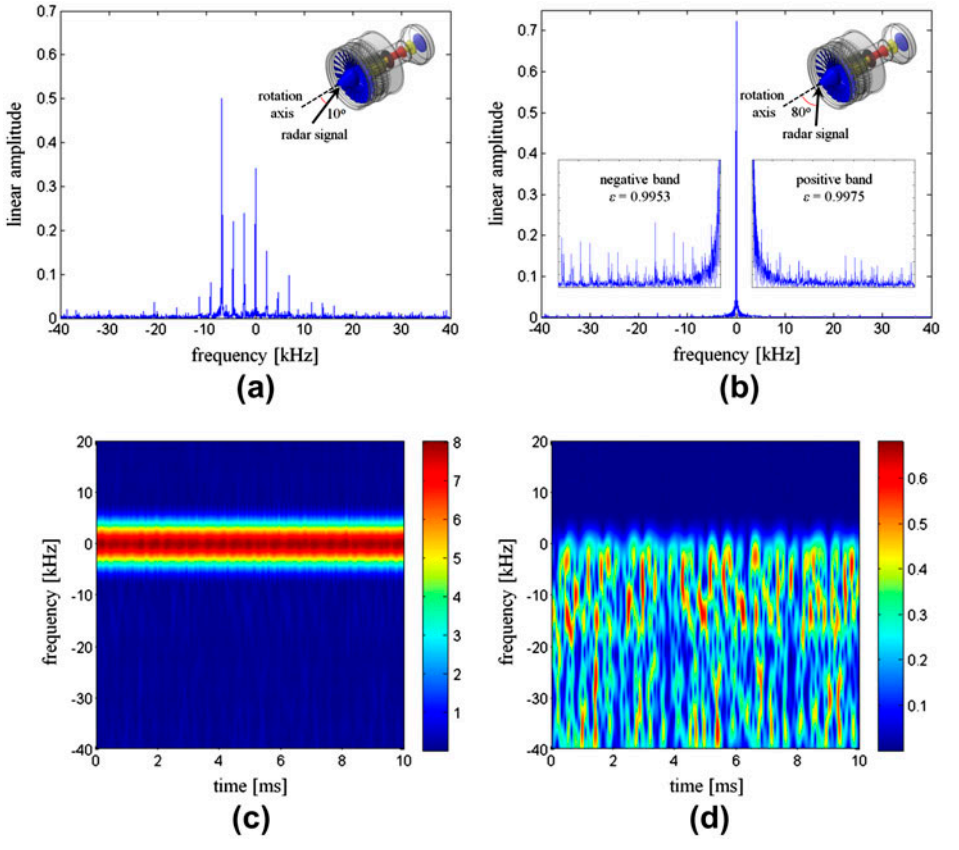

Figure 4. (a) Spectrum of simulated signal for an aspect angle of 10°, (b) spectrum of simulated signal for an aspect angle of 80° (denoted by the geometry with the CAD model), (c) spectrogram of the raw signal in (b) and (d) spectrogram of $r_9(t)$ derived from CEMD.

that the JEM spectral lines are more distinct in the negative band than in the positive band. In accordance with this observation, the eccentricity of the negative analytic form is less than that of the positive one. After decomposing the negative form using CEMD, we select $r_9(t)$ with the minimum eccentricity value. Although the spectrogram of the original signal in Figure 4(c) shows an almost constant frequency, Figure 4(d) exhibits the time-dependent JEM component. In the next section, we verify the proposed extraction method using the measured signals.

3. Verification of the proposed extraction method

3.1. *Description of examined measured raw signals*

In [3], the experimental jet engine was fabricated as shown in Figure 5 and measurement was conducted using the instrumentation radar system for various radar aspect angles and engine rotation speeds. Table 1 summarizes the information on the jet engine model and measurement parameters. Because the jet engine was not installed on the aircraft, the JEM component may be shadowed by the zero-Doppler component returned from the stationary outer wall enclosing the engine.

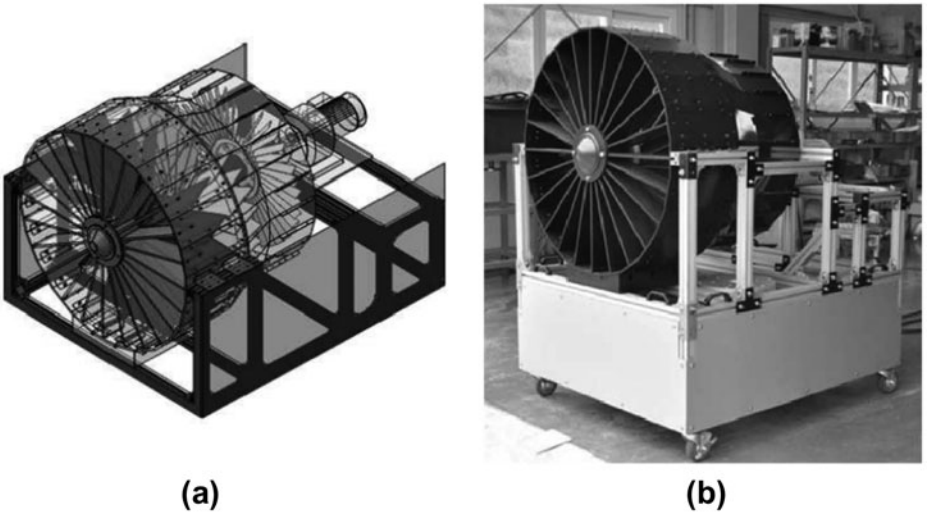

Figure 5. Experimental jet engine model. (a) CAD model, and (b) photograph.

Table 1. Information on the jet engine model and relevant measurement parameters.

Parameters	Value		
Number of rotor stages		3	
Number of blades in each stage	17	29	41
Blade length in each stage	0.385 m	0.325 m	0.300 m
Radar carrier frequency		10 GHz	
Pulse repetition frequency (PRF)		1.8 kHz	
Dwell time		2.67 s	
Rotation speeds		60.1 RPM, 180.7 RPM	
Radar incident angle		60°	

Among the measured signals, we selected two signals with different rotating speeds and a fixed radar aspect angle of 60°. As shown in Figure 6(a) and (b), these signals commonly have the dominant zero-Doppler component with an amplitude of at least 15 dB greater than those of other spectral lines. At 180.7 RPM, we selected the positive $s_a(t)$ since its eccentricity of 0.961 was less than that of the negative one of 0.980. At 60.1 RPM, the positive form was also selected as described in Section 2.2. From Figure 6(c) and (d), we find that the analytic form has more improved circularity than the raw signal. However, the JEM component should be further extracted since the analytic form still deviates from the central axis of the complex plane.

3.2 *Extraction of the weak JEM component with the proposed method*

Figure 7 shows the spectrogram and the autocorrelation of the 60.1 RPM signal. As predicted from Figure 6(a), the spectrogram shows an almost constant frequency line. Furthermore, it is difficult to observe the typical periodicity of the JEM [1] from the autocorrelation. Figure 8 exhibiting the spectrogram and the autocorrelation of the 180.7 RPM signal does not provide any useful information because the time-dependent JEM component is buried in the strong zero-Doppler component.

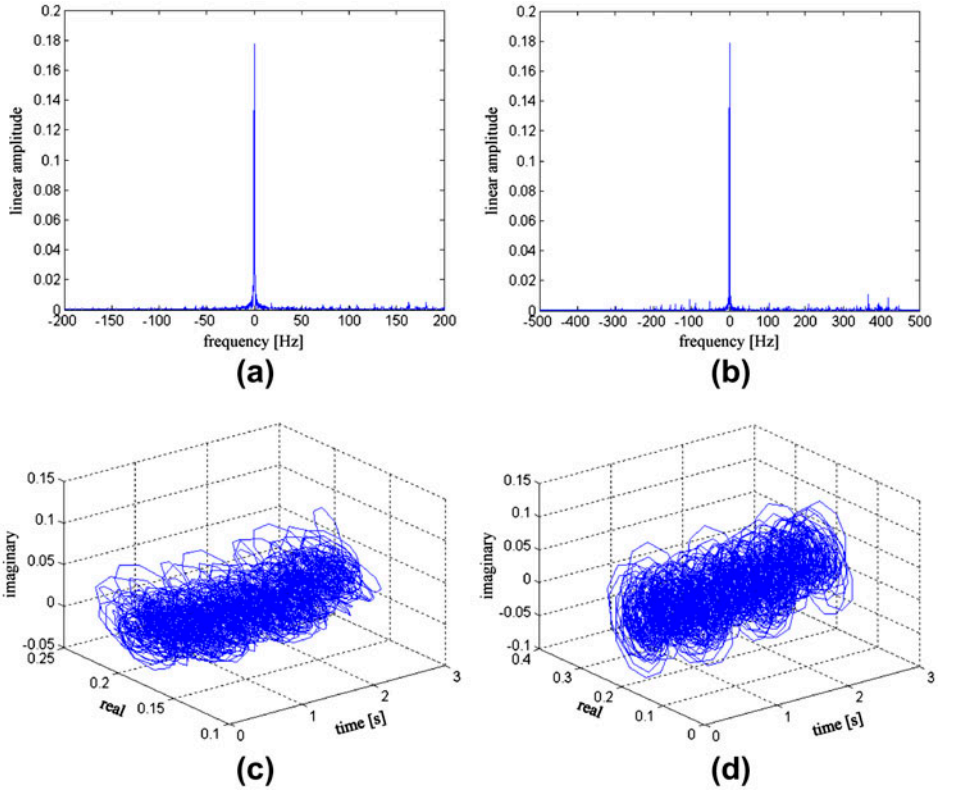

Figure 6. (a) Spectrum of measured signal of 60.1 RPM, (b) spectrum of measured signal of 180.7 RPM, (c) rotating behavior of raw signal with 60.1 RPM and (d) improved rotating behavior of positive analytic form of (c).

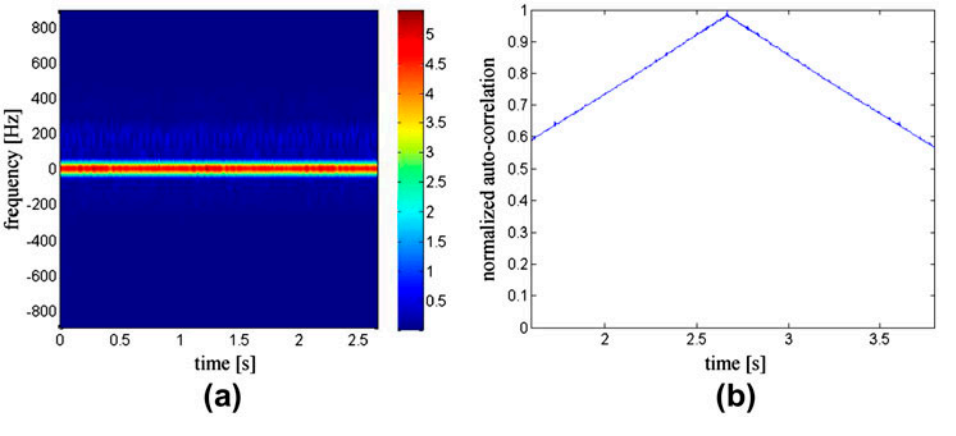

Figure 7. Measured raw signal of 60.1 RPM. (a) Spectrogram and (b) autocorrelation.

To make the JEM characteristics more discernible, we applied the CEMD with 64 directions to the analytic forms of measured signals and 10 complex IMFs were

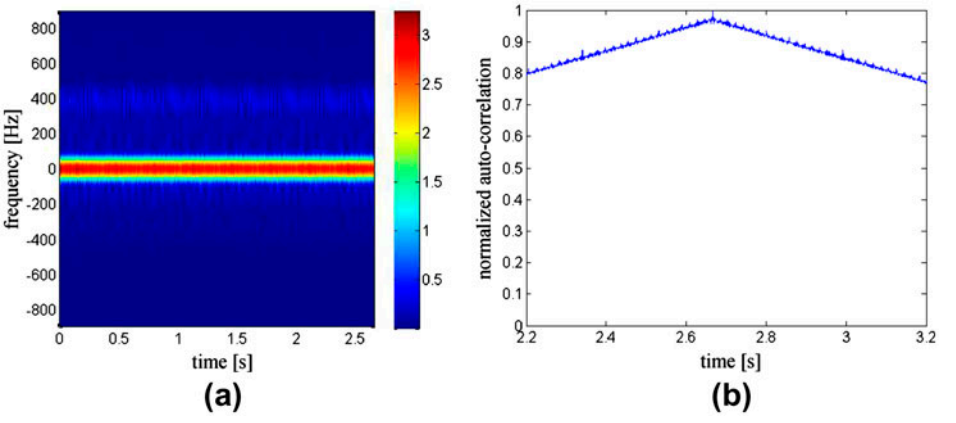

Figure 8. Measured raw signal of 180.7 RPM. (a) Spectrogram and (b) autocorrelation.

Table 2. Number of zero-crossings of each IMF for two cases of rotation speeds.

Speed	$c_1(t)$	$c_2(t)$	$c_3(t)$	$c_4(t)$	$c_5(t)$	$c_6(t)$	$c_7(t)$	$c_8(t)$	$c_9(t)$	$c_{10}(t)$
60.1	1289	719	403	229	125	73	42	24	16	0
180.7	2198	1214	675	374	214	123	65	33	16	0

extracted for each case of the rotation speed. Before calculating signal eccentricity, the number of zero-crossings of each IMF is summarized in Table 2 to compare with the proposed criterion. As the IMF order increases, the number of zero-crossings rapidly decreases. However, it is difficult to conclude which IMFs should be included for reconstructing the JEM component because there is no drastic change in the regularly decreasing zero-crossing numbers as shown in Figure 9. Thus, the minimum eccentricity condition is adopted as another standard for IMF combination. In Table 3 with the eccentricity values of $r_n(t)$, the drastic increase in the eccentricity value of $r_{10}(t)$

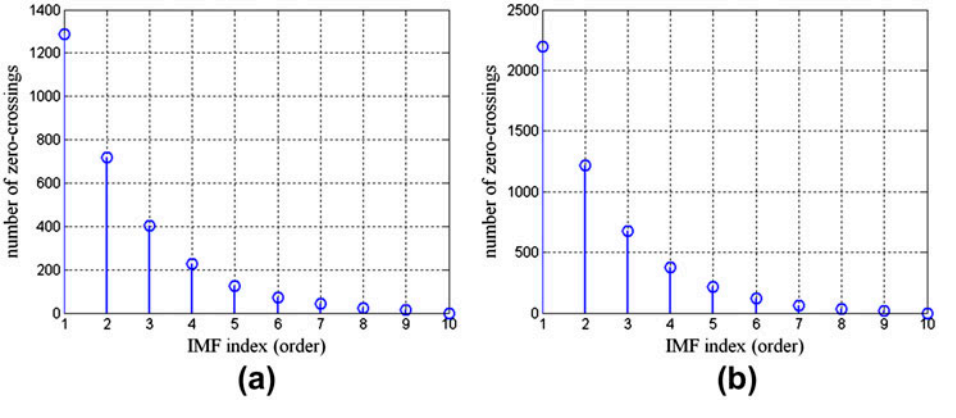

Figure 9. Number of zero-crossing of each extracted IMF. (a) 60.1 RPM signal and (b) 180.7 RPM signal.

Table 3. Eccentricity values of IMF combinations for two cases of rotation speeds.

Speed	$r_1(t)$	$r_2(t)$	$r_3(t)$	$r_4(t)$	$r_5(t)$	$r_6(t)$	$r_7(t)$	$r_8(t)$	$r_9(t)$	$r_{10}(t)$
60.1	0.121	0.087	0.073	0.056	0.047	0.029	0.018	0.037	0.053	0.972
180.7	0.048	0.089	0.064	0.057	0.056	0.038	0.029	0.017	0.022	0.961

quantitatively demonstrates that the last 10th IMF contains a strong non-rotating component. In the case of 60.1 RPM, $r_7(t)$ is regarded as best representative of the JEM component based on the minimum eccentricity condition. Figure 10(a) and (b) show the spectrogram of $r_7(t)$ where the shadowed JEM component comes into view. The spool rate, the full rotation period, can be found using the periodically repeating partial group [5] marked in Figure 10(a). The chopping rate, the period when a blade moves to its adjacent position, is estimated from the expanded spectrogram in Figure 10(b). Although the Doppler span is connected to the blade length and the rotation speed,[4] more advanced techniques for estimating the instantaneous frequency are required. Apart from the spectrogram, more intuitive JEM analysis is achieved by autocorrelation. As depicted in Figure 10(c) and (d), the number of blades in the first rotor stage can be obtained as 17 using the spool rate between the outstanding 'spool peaks' and the chopping rate between the surrounding 'chopping peaks'. Note that the turbine blades in the front stage make the primary contribution to the JEM effect.[1–3]

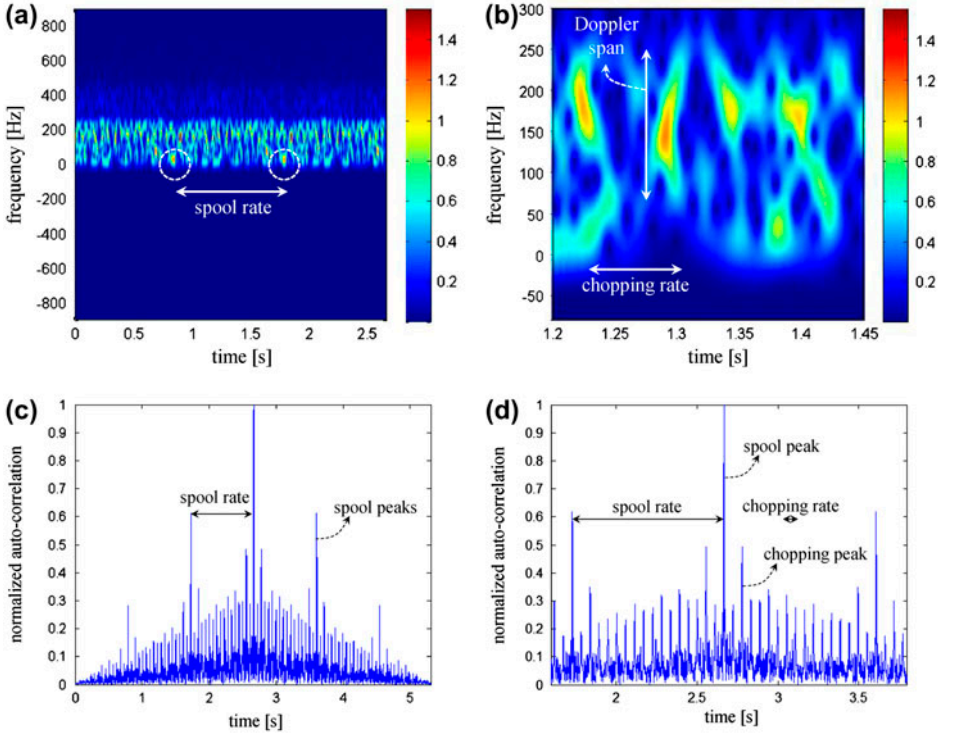

Figure 10. Results of JEM component extraction at 60.1 RPM. (a) Spectrogram of $r_7(t)$, (b) expanded between 1.2 and 1.45 s, (c) autocorrelation of $r_7(t)$, and (d) expanded with respect to the maximum peak.

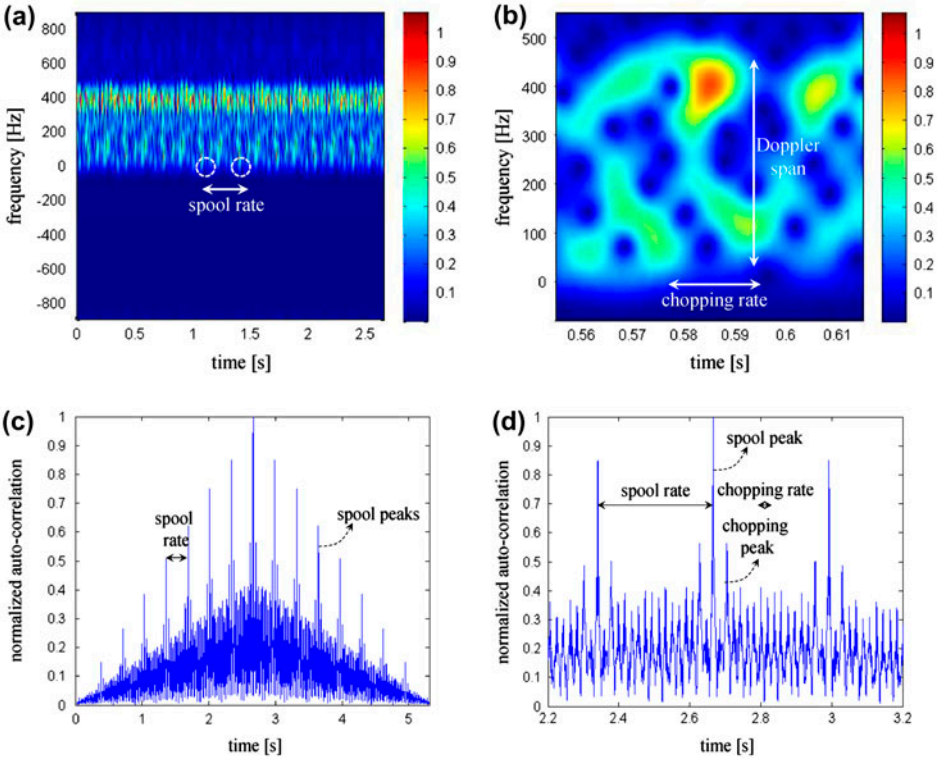

Figure 11. Results of JEM component extraction 180.7 RPM. (a) Spectrogram of $r_8(t)$, (b) expanded between 0.55 and 0.61 s, (c) autocorrelation of $r_8(t)$, and (d) expanded with respect to the maximum peak.

When the rotation speed increases to 180.7 RPM, $r_8(t)$ is designated as the extracted JEM component according to Table 3, and Figure 11 presents its spectrogram and autocorrelation. The spectrogram helps us obtain the information on the jet engine, such as the spool rate, the chopping rate, and the Doppler span spread by the increased rotation speed. The autocorrelation suggests that the body returned component was effectively removed and the number of blades in the first rotor stage can be estimated precisely. In conclusion, examination with measured raw signals confirmed that the clarity of the JEM analysis was significantly improved by the proposed method.

4. Conclusion and discussion

In this study, we presented a method for extracting the weakly present JEM component. To relieve the complexity of the signal, it was transformed into the analytic form. After decomposing the analytic form into several IMFs using CEMD, the signal eccentricity facilitated effective reconstruction of the JEM component by indicating the desirable IMF combination. Consequently, the clarity of the JEM analysis was significantly improved and the proposed method is expected to be useful for enhanced radar target recognition. Future studies will focus on application to signals measured from aircraft targets where the JEM component may be shadowed by the real aircraft structures.

More sophisticated algorithms are also under investigation to estimate instantaneous frequencies from the joint time-frequency domain. In addition, the drawbacks of CEMD caused by noise should be discussed. In this paper and [12,17], CEMD was employed as a kind of 'denoising' methods to remove unwanted frequency components. However, for the white Gaussian noise, CEMD becomes highly sensitive to it since decomposition of CEMD is performed based on the distribution of local extrema.[24] The analyzed signal cannot clearly contain rotating components by the white noise, and thus, the IMF may wander around the central axis of the complex plane in a complicated way.[16] Therefore, other insensitive methods, such as chirplet decomposition [15] should be employed for preprocessing the raw noise-corrupted signal.

Acknowledgement

This research was supported by the Agency for Defense Development.

References

[1] Bell MR, Grubbs RA. JEM modeling and measurement for radar target identification. IEEE Trans. Aerosp. Electron. Syst. 1993;29:73–87.
[2] Tait, P. Introduction to radar target recognition. Vol. 18, IET Radar, Sonar and Navigation Series. London: Institution of Engineering and Technology (IET); 2005.
[3] Lim H, Yoo JH, Kim CH, Kwon KI, Myung NH. Radar cross section measurements of a realistic jet engine structure with rotating parts. J. Electromagn. Waves Appl. 2011;25:999–1008.
[4] Lim H, Park JH, Yoo JH, Kim CH, Kwon KI, Myung NH. Joint time-frequency analysis of radar micro-Doppler signatures from aircraft engine models. J. Electromagn. Waves Appl. 2011;25:1069–1080.
[5] Park JH, Lim H, Myung NH. Analysis of jet engine modulation effect with extended Hilbert-Huang transform. Electron. Lett. 2013;49:215–216.
[6] Woo JC, Lim BG, Kim YS. Modification of the recursive sidelobe minimization technique for the range-Doppler algorithm of SAR imaging. J. Electromagn. Waves Appl. 2011;25:1783–1794.
[7] Park SH. Automatic recognition of targets in formation using range profiles. J. Electromagn. Waves Appl. 2012;26:2059–2069.
[8] Thayaparan T, Abrol S, Riseborough E, Stankovic L, Lamothe D, Duff G. Analysis of radar micro-Doppler signatures from experimental helicopter and human data. IET Radar Sonar Navig. 2007;1:289–299.
[9] Thayaparan T, Suresh P, Qian S, Venkataramaiah K, SivaSankaraSai S, Sridharan KS. Micro-Doppler analysis of a rotating target in synthetic aperture radar. IET Radar Sonar Navig. 2010;4:245–255.
[10] Stankovic L, Djurovic I, Thayaparan T. Separation of target rigid body and micro-Doppler effect in ISAR imaing. IEEE Trans. Aerosp. Electron. Syst. 2006;42:1496–1506.
[11] Zhang Q, Yeo TS, Tan HS, Luo Y. Imaging of a moving target with rotating parts based on the Hough transform. IEEE Trans. Geosci. Remote Sens. 2008;46:291–299.
[12] Bai X, Xing M, Zhou F, Lu G, Bao Z. Imaging of micromotion targets with rotating parts based on empirical mode decomposition. IEEE Trans. Geosci. Remote Sens. 2008;46:3514–3523.
[13] Li P, Wang D, Wang L. Separation of micro-Doppler signals based on time frequency filter and Viterbi algorithm. Signal Image Video Process. 2011;7:593–605.
[14] Stankovic L, Thayaparan T, Dakovic M, Popovic-Bugarin V. Micro-Doppler removal in the radar imaging analysis. IEEE Trans. Aerosp. Electron. Syst. 2013;49:1234–1250.
[15] Jung JH, Kim KT, Park SH. Removal of JEM signal by accurate estimation of initial parameters of chirplet basis functions. Prog. Electromagn. Res. 2013;141:607–618.
[16] Rilling G, Flandrin P, Goncalves P, Lilly JM. Bivariate empirical mode decomposition. IEEE Signal Process Lett. 2007;14:936–939.

[17] Zhou F, Xing M, Bai X, Sun G, Bao Z. Narrow-band interference suppression for SAR based on complex empirical mode decomposition. IEEE Geosci. Remote Sens. Lett. 2009;6:423–427.
[18] Yang W, Court R, Tavner PJ, Crabtree CJ. Bivariate empirical mode decomposition and its contribution to wind turbine condition monitoring. J. Sound Vib. 2011;330:3766–3782.
[19] Rilling G, Flandrin P. One or two frequencies? The empirical mode decomposition answers. IEEE Trans. Signal Process. 2008;56:85–95.
[20] Yunchao G, Enfang S, Baifeng L, Zhengyan S. Application of complex empirical mode decomposition for unbalanced real-world signals. IEEE International Conference Neural Network and Signal Processing Proceeding; 2008 Jun; 294–298; Zhenjian, China.
[21] Ollila E. On the circularity of a complex random variable. IEEE Signal Process Lett. 2008;15:841–844.
[22] Ahrabian A, Rehman NU, Mandic D. Bivariate empirical mode decomposition for unbalanced real-world signals. IEEE Signal Process Lett. 2013;20:245–248.
[23] Huang NE, Shen Z, Long SR, Wu MC, Shih HH, Zheng Q, Yen NC, Tung CC, Liu HH. The empirical mode decomposition and the Hilbert spectrum for nonlinear and non-stationary time series analysis. Proc. R. Soc. A. 1998;454:903–995.
[24] Wu Z, Huang NE. Ensemble empirical mode decomposition: a noise-assisted data analysis method. Adv. Adaptive Data Anal. 2009;1:1–41.